Optical forces exerted on a graphene-coated dielectric particle by a focused Gaussian beam

Yang Yang,[1,2,†] Zhe Shi,[1,†] Jiafang Li,[1,*] and Zhi-Yuan Li[1]

[1]*Laboratory of Optical Physics, Institute of Physics, Chinese Academy of Sciences, P.O. Box 603, Beijng 100190, China*
[2]*Key Laboratory of Micro-Nano Measurement-Manipulation and Physics (Ministry of Education), Beihang University, Beijing 100191, China*
**Corresponding author: jiafangli@aphy.iphy.ac.cn*

Received December 14, 2015; revised February 21, 2016; accepted February 21, 2016; posted February 24, 2016 (Doc. ID 255644); published March 21, 2016

In this paper, we derive the analytical expression for the multipole expansion coefficients of scattering and interior fields of a graphene-coated dielectric particle under the illumination of an arbitrary optical beam. By using this arbitrary beam theory, we systematically investigate the optical forces exerted on the graphene-coated particle by a focused Gaussian beam. Via tuning the chemical potential of the graphene, the optical force spectra could be modulated accordingly at resonant excitation. The hybridized whispering gallery mode of the electromagnetic field inside the graphene-coated polystyrene particle is more intensively localized than the pure polystyrene particle, which leads to a weakened morphology-dependent resonance in the optical forces. These investigations could open new perspectives for dynamic engineering of optical manipulations in optical tweezers applications.

OCIS codes: (350.4855) Optical tweezers or optical manipulation; (140.7010) Laser trapping; (250.5403) Plasmonics; (170.4520) Optical confinement and manipulation.
http://dx.doi.org/10.1364/PRJ.4.000065

1. INTRODUCTION

Since Ashkin *et al.* proved the possibility of trapping a dielectric particle by a focused light beam [1], the manipulation of microscopic particles with optical tweezers has attracted increasing interest and attention, where the results have consolidated the importance of this technology in several fields. The optical tweezers have been used to manipulate and trap microscale objects [1], liquid droplets [2], metal nanoparticles [3], magneto dielectric particles [4], nanostructures [5], Janus particles [6], and even some submicrometer objects such as cells and viruses [7] without mechanical contact. The family of microscopic objects under study of optical tweezers has steadily expanded.

Recently, graphene, which is composed of a single layer of carbon atoms, has attracted intensive investigation [8–10] due to its excellent optical properties [11,12]. Graphene also shows remarkable effects when the material interacts with split-ring resonator-based metamaterials [13], nanoantennas [14,15], Brownian motion [16], on-chip optical modulators [17], and localized surface plasmons [18], and it is promised as a novel platform for integrated optoelectronics and transformation optics [19,20].

Recently, interest has emerged also in exploring the properties of light-plasmon interaction in curved configurations, e.g., bent and corrugated sheets [21,22], cloaking structures [23], and various coated nanowire systems [24,25]. The spherical geometry is also of experimental relevance, given recent fabrication demonstrations [26]. Notably, one could electrically control plasmonic resonances in gold nanorods [27].

In view of the excellent optical properties of graphene, in this work, we apply it to the conventional optical tweezers via graphene-coated dielectric nanoparticles. Here, we report our systematic study on the optical forces exerted on a graphene-coated spherical particle by a focused Gaussian beam by utilizing the arbitrary beam theory (ABT). The detailed results and discussions are shown as follows.

2. THEORETICAL DESCRIPTION

Within the Mie scattering problem, the general electromagnetic wave scalar potential can be expanded as a series expression in vector wave functions, e.g., for the incident field, the expansion is [28]

$$\Pi_E^{(i)} = \sum_{l=1}^{\infty}\sum_{m=-l}^{l} A_{lm}\psi_l(k_1 r)Y_{lm}(\theta,\phi),$$
$$\Pi_H^{(i)} = \sum_{l=1}^{\infty}\sum_{m=-l}^{l} B_{lm}\psi_l(k_1 r)Y_{lm}(\theta,\phi), \quad (1)$$

the expansion for the scattered field:

$$\Pi_E^{(s)} = \sum_{l=1}^{\infty}\sum_{m=-l}^{l} a_l A_{lm}\xi_l^{(1)}(k_1 r)Y_{lm}(\theta,\phi),$$
$$\Pi_H^{(s)} = \sum_{l=1}^{\infty}\sum_{m=-l}^{l} b_l B_{lm}\xi_l^{(1)}(k_1 r)Y_{lm}(\theta,\phi), \quad (2)$$

and the expansion for the internal field:

$$\Pi_E^{(w)} = \sum_{l=1}^{\infty}\sum_{m=-l}^{l} c_l A_{lm}\psi_l(k_2 r)Y_{lm}(\theta,\phi),$$
$$\Pi_H^{(w)} = \sum_{l=1}^{\infty}\sum_{m=-l}^{l} d_l B_{lm}\psi_l(k_2 r)Y_{lm}(\theta,\phi). \quad (3)$$

The superscript of the scalar potentials for incident field is designated by (i), the scattered field by (s), and the internal

field is designated by (w), respectively. θ is the polar angle and ϕ is the azimuthal angle; $\xi_l^{(1)} = \psi_l - i\chi_l$, ψ_l and χ_l are the Riccati–Bessel functions. $k_0 = \omega/c$ is the wavenumber in vacuum. k_1 and k_2 are the wave vector inside and outside the particle. R is the particle radius. The spherical harmonics are

$$Y_{lm}(\theta,\phi) = \left[\frac{2l+1}{4\pi}\frac{(l-m)!}{(l+m)!}\right]^{1/2} P_l^m(\cos\theta)\exp(im\phi). \quad (4)$$

The expansion coefficients for the incident electromagnetic field in ABT are

$$A_{lm} = \frac{1}{l(l+1)\psi_l(\alpha_2)}\int_0^{2\pi}\int_0^{\pi} E_r^{(i)}(R,\theta,\phi)Y_{lm}^*(\theta,\phi)\sin\theta \mathrm{d}\theta\mathrm{d}\phi,$$
$$B_{lm} = \frac{1}{l(l+1)\psi_l(\alpha_2)}\int_0^{2\pi}\int_0^{\pi} H_r^{(i)}(R,\theta,\phi)Y_{lm}^*(\theta,\phi)\sin\theta \mathrm{d}\theta\mathrm{d}\phi, \quad (5)$$

where $\alpha_2 = k_2 R$.

Using the local-response approximation (LRA), both the scalar potentials for electric field Π_E and the magnetic field Π_H satisfy the homogeneous Helmholtz wave equation:

$$\nabla^2\Pi + k^2\Pi = 0. \quad (6)$$

The corresponding electromagnetic field satisfies the condition of Eq. (6), which can be derived through the Maxwell equations directly [28].

Here, the graphene coating can be considered as a surface current $\mathbf{K}$ around the spherical dielectric particle. The boundary conditions at the domain-interface of $r = R$ are as follows: the tangential component of the total electric field E is continuous and the discontinuity of the tangential component of the total magnetic field H is proportional in magnitude to the surface current density; thus, the boundary conditions can be expressed as

$$\mathbf{e}_r \times (\mathbf{E}_i + \mathbf{E}_s - \mathbf{E}_w) = 0$$
$$\mathbf{e}_r \times (\mathbf{H}_i + \mathbf{H}_s - \mathbf{H}_w) = \mathbf{K} = \sigma(\omega)\mathbf{E}_{\|}, \quad (7)$$

where $\mathbf{e}_r$ is the associated normal vector, $\mathbf{E}_{\|}$ is the tangential component of the total electric field. The complex surface electrical conductivity of graphene $\sigma(\omega)$ is calculated with the random-phase approximation (RPA) in the local limit from the Kubo formula [29,30], including the interband and intraband transition contributions:

$$\sigma(\omega) = \sigma_{\mathrm{intra}}(\omega) + \sigma_{\mathrm{inter}}(\omega). \quad (8)$$

Apart from the angular frequency ω, the value of $\sigma(\omega)$ depends on the Fermi level of graphene E_f, temperature T, and carrier relaxation time τ in graphene. For the intraband $\sigma_{\mathrm{intra}}(\omega)$ and interband $\sigma_{\mathrm{inter}}(\omega)$ contributions, we have used the following expressions:

$$\sigma_{\mathrm{intra}}(\omega) = \frac{i2e^2k_BT}{\pi\hbar^2(\omega + i\tau_{\mathrm{G}}^{-1})}\ln\left[2\cosh\left(\frac{E_f}{2k_bT}\right)\right], \quad (9)$$

$$\sigma_{\mathrm{inter}}(\omega) = \frac{e^2}{4\hbar}\left[\begin{array}{l}\frac{1}{2} + \frac{1}{\pi}\arctan\left(\frac{\hbar\omega - 2E_f}{2k_BT}\right) \\ -\frac{i}{2\pi}\ln\frac{(\hbar\omega+2E_f)^2}{(\hbar\omega-2E_f)^2+4k_b^2T^2}\end{array}\right], \quad (10)$$

where k_B is Boltzmann constant, $\hbar$ is the reduced Planck constant. In all the calculations, we have used $T = 300$ K (room temperature), and graphene's mobility with 10000 $\mathrm{cm}^2/(\mathrm{V}\cdot\mathrm{s})$, which are commonly used in many calculations. The spherical particle's permittivity can be tuned by changing the surface conductivity of graphene $\sigma(\omega)$, which have the relationship: $\varepsilon = 1 + i[\sigma(\omega)/\omega\varepsilon_0 R]$.

Finally, enforcing the boundary conditions translated into local, linear continuum relations between the incident and scattered amplitudes, the multipole expansion coefficients of the scattered electromagnetic field by the graphene coated particle are obtained as

$$a_l = -[\tilde{n}\psi_l(\alpha_1)\psi_l'(\alpha_2) - \psi_l(\alpha_2)\psi_l'(\alpha_1) + (1/n_2)\sigma(\omega) \cdot \psi_l'(\alpha_1)\psi_l'(\alpha_2)]/[\tilde{n}\psi_l(\alpha_1)\xi_l'(\alpha_2) - \xi_l^{(1)}(\alpha_2)\psi_l'(\alpha_1) + (1/n_2)\sigma(\omega)\cdot\psi_l'(\alpha_1)\xi_l'(\alpha_2)], \quad (11)$$

$$b_l = -[\tilde{n}\psi_l'(\alpha_1)\psi_l(\alpha_2) - \psi_l(\alpha_1)\psi_l'(\alpha_2) + (1/n_2)\sigma(\omega) \cdot \psi_l(\alpha_1)\psi_l(\alpha_2)]/[\tilde{n}\psi_l'(\alpha_1)\xi_l(\alpha_2) - \psi_l(\alpha_1)\xi_l^{(1)\prime}(\alpha_2) + (1/n_2)\sigma(\omega)\cdot\psi_l(\alpha_1)\xi_l(\alpha_2)], \quad (12)$$

where $\alpha_1 = k_1 R, \tilde{n} = n_1/n_2$. Also, by adopting the boundary conditions of the linear continuum relations between the incident and internal amplitudes, the multipole expansion coefficients of the interior electromagnetic field inside the particle are derived as

$$c_l = \tilde{n}[\psi_l(\alpha_2)\xi_l'(\alpha_2) - \psi_l'(\alpha_2)\xi_l^{(1)}(\alpha_2)]/[\tilde{n}\psi_l(\alpha_1)\xi_l'(\alpha_2) - \xi_l^{(1)}(\alpha_2)\psi_l'(\alpha_1) + (1/n_2)\sigma(\omega)\cdot\psi_l'(\alpha_1)\xi_l'(\alpha_2)], \quad (13)$$

$$d_l = [\psi_l'(\alpha_2)\xi_l(\alpha_2) - \psi_l(\alpha_2)\xi_l^{(1)\prime}(\alpha_2)]/[\tilde{n}\psi_l'(\alpha_1)\xi_l(\alpha_2) - \psi_l(\alpha_1)\xi_l^{(1)\prime}(\alpha_2) + (1/n_2)\sigma(\omega)\cdot\psi_l(\alpha_1)\xi_l(\alpha_2)]. \quad (14)$$

The optical force $\mathbf{F}$ exerted on the spherical particle illuminated by the electromagnetic wave can be expressed as a series over the coefficients A_{lm}, B_{lm}, a_{lm}, and b_{lm} [31]. Here, we redefine

$$a_{lm} = a_l A_{lm}, b_{lm} = b_l B_{lm}.$$

3. RESULTS AND DISCUSSION

The schematic of scattering is shown in Fig. 1. Here, the graphene-coated polystyrene spherical particle is considered as a two-component spherically symmetric system, coinciding at the origin of the coordinate and coated by a conductive film at the interface. The ambient medium is vacuum. A focused Gaussian beam with waist radius $w_0 = 2$ μm is incident upon a graphene-coated polystyrene particle with radius R. The refractive index of polystyrene particle is $n_1 = 1.59$. We take the x–z plane as the plane of incidence. The Gaussian beam is p polarized, the beam center is at (x_0, y_0, z_0). The input power $P = 10$ mW.

Figure 2 depicts the vertical optical force F_z exerted on a graphene-coated polystyrene particle by a focused Gaussian beam as a function of wavelength with the variation of particle radius R (while the Fermi energy is fixed as $E_f = 0.6$ eV)

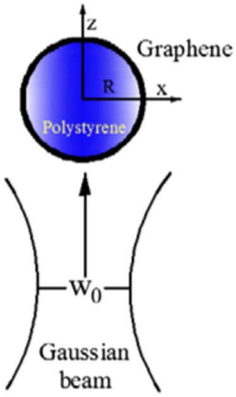

Fig. 1. Focused Gaussian beam with waist radius w_0 is incident upon a graphene-coated polystyrene spherical particle with radius R.

[Fig. 2(a)] and Fermi energy E_f (while the particle radius is fixed as $R = 50$ nm) [Fig. 2(b)]. Figures 2(c) and 2(d) plot the wavelength of the resonance peak with the variation of particle radius and the Fermi energy, respectively. The mathematical description of the electromagnetic field of Gaussian beam for the evaluation of the integrals is given in [32].

It is observed in Figs. 2(a) and 2(c) that, with the increase of particle size, the corresponding wavelength of resonant peak increases gradually. The optical force peaks are formed from the plasmonic resonances, which are mainly generated by dipole contribution in the analysis. In Figs. 2(b) and 2(d), with the Fermi energy E_f increased (this can be quantified through chemical doping of different level), the wavelength of the resonant peak decreases accordingly.

In addition, the optical forces on graphene-coated particles can be further controlled by the surface conductivity, which is determined by the chemical potential that can be tuned with the help of the gate voltage or doping. Figure 3 presents the optical forces as a function of the displacement of the beam center along the x axis on a graphene-coated polystyrene spherical particle with radius $R = 50$ nm at resonant wavelength $\lambda = 5151$ nm excitation with different Fermi energy. It can be seen that the vertical force F_z reaches the maximum at the center of beam waist and the bidirectional oriented gradient force F_x would laterally pull the particle to the center of the beam spot. Furthermore, on the resonant excitation,

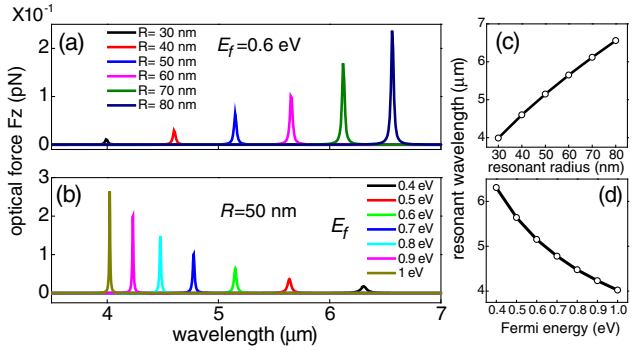

Fig. 2. Vertical optical force F_z exerted on a graphene-coated polystyrene particle by a focused Gaussian beam as a function of wavelength with different (a) particle radius and (b) Fermi energy. (c) and (d) plot the resonant wavelength as a function of particle radius and Fermi energy, respectively.

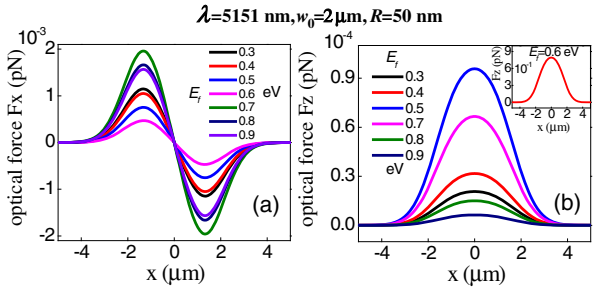

Fig. 3. Optical forces as a function of the displacement of beam center along the x axis on a graphene-coated polystyrene particle with radius $R = 50$ nm at resonant excitation wavelength $\lambda = 5151$ nm: (a) horizontal direction F_x and (b) vertical direction F_z with different Fermi energy impactions. Inset: Optical force F_z with Fermi energy $E_f = 0.6$ eV.

with the designing of Fermi energy (or the chemical potential), the optical forces along the horizontal direction F_x and vertical direction F_z can be tuned accordingly. In both cases, the changes in optical force lines with the Fermi energy are not monotonic. A maximum value of F_z at resonant Fermi energy of $E_f = 0.6$ eV is exhibited, as shown in the inset of Fig. 3(b). Due to the resonant absorption of graphene coating, the amplitude of optical force is enhanced by 3 orders of magnitude.

Then, we investigate the variation of vertical forces F_z as a function of the displacement of the beam center along z axis (beam propagating direction) in Fig. 4 with different Fermi energy: (a) off-resonance, (b) at resonant Fermi energy of $E_f = 0.6$ eV, under wavelength $\lambda = 5151$ nm, particle size $R = 50$ nm, and beam waist radius $w_0 = 0.5$ μm. The particle's horizontal position is at the beam center of $x = y = 0$.

It is shown in Fig. 4(a) that under the condition of highly focused Gaussian beam of small beam waist, the variation of vertical force F_z along the beam propagating axis also exhibits a bidirectional shape, which would trap the particle at the beam center. By tuning the Fermi energy, the corresponding adjustment of the vertical force could help to regulate the trapping stiffness of the particle for optical manipulation. In Fig. 4(b), at the absorbing resonance of the graphene layer, F_z is greatly enhanced, and the vertical force line exhibits a Lorentz shape that will pull the particle out of the beam center.

These results illustrate the advantage of graphene coating, which provides excellent control over the resonant amplitude of the optical forces via the modulation of chemical potential. Such tunability could be experimentally demonstrated and

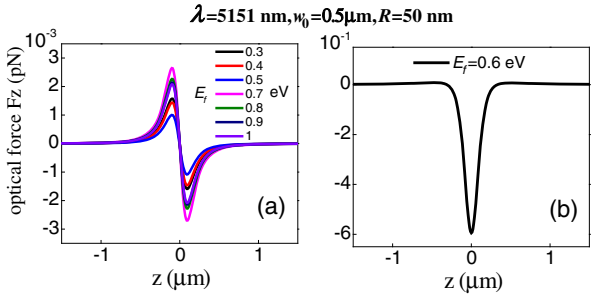

Fig. 4. Vertical forces F_z as a function of the displacement of beam center along the z axis with different Fermi energy of the graphene coating. $\lambda = 5151$ nm, $R = 50$ nm.

used to control the optical forces on manipulating the dielectric particle or the cell and explore the dynamics between matter and light in graphene [33,34]. Meanwhile, carrier concentration as high as 10^{14} cm^{-2} has been feasible, which corresponds to a chemical potential higher than 1 eV [35,36].

Figure 5 demonstrates the optical force as a function of spherical particle radius (0.9 μm $< R <$ 1.2 μm) in the case of (a) polystyrene particle, (b) graphene coated polystyrene particle, and (c) empty graphene particle (vacuum inside). The particle is placed in air, and the Fermi energy is fixed as 0.6 eV in all cases. $w_0 = 2$ μm. As we can see, the optical forces of the three kinds of particles are modulated with the increase of the particle size. The variations in optical force spectra of the polystyrene particle and graphene-coated polystyrene particle show obvious size-dependent oscillations of morphology dependent resonance (MDR) in Figs. 5(a) and 5(b). Furthermore, it is clear to see that the oscillation amplitude of MDRs of the graphene-coated polystyrene particle is smaller than the bare polystyrene particle. This weakness in resonance strength is caused by the absorption of the coated graphene.

It should be mentioned that there is no oscillation for a bare graphene spherical particle in the whole variations of particle size in Fig. 5(c). It only shows a smooth and monotonous increase of the optical forces with the increased particle radius. This is because there does not exist mutual interfering resonance of the electromagnetic wave inside the coated graphene layer. Interestingly, the MDR order of a pure polystyrene particle as shown in Fig. 5(a), the multipole expansion coefficient of the magnetic scattering wave (b_l) appears first before that of electric scattering wave (a_l). But, in Fig. 5(b), for a graphene-coated polystyrene particle, the MDR order is inverted, i.e., a_l emerges before the appearance of b_l [37,38].

In order to get deep insight into the physical difference in MDR resonant peaks between the pure polystyrene particle and graphene-coated polystyrene particle, we investigate the mutual interactions of these particles with the incident-focused Gaussian beam. Here, we show two types of representative field patterns at a multipole resonant peak of electric scattering field a_{12} in Figs. 6(a)–6(c) and magnetic scattering field b_{12} in Figs. 6(d)–6(f), respectively. The spatial distribution of the electric field magnitude |**E**| around the particle in the x–z plane (incident plane) is shown in Fig. 6.

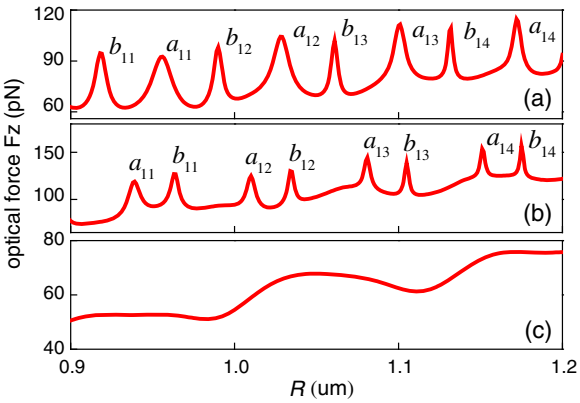

Fig. 5. Optical force as a function of the particle radius: (a) polystyrene particle; (b) graphene-coated polystyrene particle; (c) empty graphene particle.

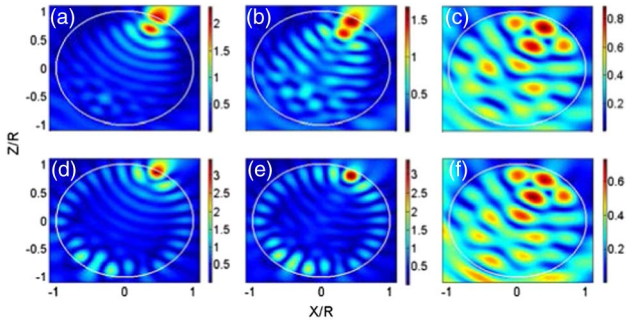

Fig. 6. WGM of electric field patterns of: (a), (d) polystyrene particle, (b), (e) graphene-coated polystyrene particle, (c), (f) bare graphene shell, at resonance of (a)–(c) electric field multipoles a_{12} and (d)–(f) magnetic multipoles b_{12}, respectively.

It is demonstrated that at MDR [with respect to the bare graphene particle shown in Figs. 6(c) and 6(f)], almost all of the incident waves are coupled into the particle on resonance, which is confined near the surface by total internal reflection. The mutual interference of the internal traveling wave leads to a lap of bright spots along the surface on resonance. As clearly shown in Figs. 6(d) and 6(e), the occurrence of the multipole resonant peak accompany a corresponding whispering gallery mode (WGM) interior field structure, which is also applicable for a graphene-coated dielectric particle. Taking into account that the WGM is generated on the magnetic multipole b_{12} resonance, the MDR here is mainly contributed by the resonance of a magnetic multipole scattering wave coefficient b_l.

Essentially, the WGM pattern of the polystyrene particle and the hybridized WGM pattern of the graphene-coated polystyrene particle on resonance of b_{12} are almost the same. However, due to the electromagnetic coupling between the WGMs of the polystyrene particle [Fig. 6(d)] and the internally localized modes of the bare graphene coating [Fig. 6(f)], the hybridized internal modes in the graphene-coated polystyrene particle almost cannot penetrate outside the particle regions and is confined within a surface layer of approximately one skin depth in thickness. This means that the hybridized WGMs of the graphene-coated particle are more intensively localized than those of the pure polystyrene particle, which leads to a weakened MDR oscillation in the optical forces [Fig. 5(b)].

4. CONCLUSIONS

In summary, we obtained the analytical expressions for multipole scattering and interior field expansion coefficients of a graphene-coated particle with ABT. Based on these derivations, we systematically investigated the optical forces exerted on a graphene-coated particle by a focused Gaussian beam and compared the results with a Mie dielectric particle. We found that the hybridized WGMs of the graphene-coated particle are more localized due to the mutual electromagnetic coupling between the WGMs of the pure dielectric particle and internally localized modes of the pure graphene coating; as a result, the corresponding MDR oscillation is weakened for the graphene-coated particle. With the tunability in optical properties of graphene, our investigations could open new perspectives for dynamic engineering of optical manipulations in optical tweezer techniques.

ACKNOWLEDGMENT

This work is supported by the National 973 Program of China (Nos. 2013CB632704 and 2013CB922404), and the National Natural Science Foundation of China (Nos. 11374357, 61475186, and 11434017).

† These authors contributed equally to this work.

REFERENCES

1. A. Ashkin, J. M. Dziedzic, J. E. Bjorkholm, and S. Chu, "Observation of a single-beam gradient force optical trap for dielectric particles," Opt. Lett. **11**, 288–290 (1986).
2. P. H. Jones, E. Stride, and N. Saffari, "Trapping and manipulation of microscopic bubbles with a scanning optical tweezer," Appl. Phys. Lett. **89**, 081113 (2006).
3. L. Bosanac, T. Aabo, P. M. Bendix, and L. B. Oddershede, "Efficient optical trapping and visualization of silver nanoparticles," Nano Lett. **8**, 1486–1491 (2008).
4. M. Nieto-Vesperinas and J. J. Saenz, "Optical forces from an evanescent wave on a magnetodielectric small particle," Opt. Lett. **35**, 4078–4080 (2010).
5. O. M. Maragò, P. H. Jones, P. G. Gucciardi, G. Volpe, and A. C. Ferrari, "Optical trapping and manipulation of nanostructures," Nat. Nanotechnol. **8**, 807–819 (2013).
6. Y. W. Zong, J. Liu, R. J. Liu, H. L. Guo, M. C. Yang, Z. Y. Li, and K. Chen, "An optically driven bistable Janus rotor with patterned metal coatings," ACS Nano **9**, 10844–10851 (2015).
7. A. Ashkin and J. M. Dziedzic, "Optical trapping and manipulation of viruses and bacteria," Science **235**, 1517–1520 (1987).
8. K. S. Novoselov, A. K. Geim, S. V. Morozov, D. Jiang, M. I. Katsnelson, I. V. Grigorieva, S. V. Dubonos, and A. A. Firsov, "Two-dimensional gas of massless Dirac fermions in graphene," Nature **438**, 197–200 (2005).
9. Z. Q. Li, E. A. Henriksen, Z. Jiang, Z. Hao, M. C. Martin, P. Kim, H. L. Stormer, and D. N. Basov, "Dirac charge dynamics in graphene by infrared spectroscopy," Nat. Phys. **4**, 532–535 (2008).
10. M. Bruna and S. Borini, "Optical constants of graphene layers in the visible range," Appl. Phys. Lett. **94**, 031901 (2009).
11. P. Y. Chen and A. Alù, "Atomically thin surface cloak using graphene monolayers," ACS Nano **5**, 5855–5863 (2011).
12. J. S. Gómez-Díaz and J. Perruisseau-Carrier, "Propagation of hybrid transverse magnetic transverse electric plasmons on magnetically biased graphene sheets," J. Appl. Phys. **112**, 124906 (2012).
13. N. Papasimakis, Z. Luo, Z. X. Shen, F. D. Angelis, E. D. Fabrizio, A. E. Nikolaenko, and N. I. Zheludev, "Graphene in a photonic metamaterial," Opt. Express **18**, 8353–8359 (2010).
14. Z. Fang, Z. Liu, Y. Wang, P. M. Ajayan, P. Nordlander, and N. J. Halas, "Graphene-antenna sandwich photodetector," Nano Lett. **12**, 3808–3813 (2012).
15. T. J. Echtermeyer, L. Britnell, P. K. Jasnos, A. Lombardo, R. V. Gorbachev, A. N. Grigorenko, A. K. Geim, A. C. Ferrari, and K. S. Novoselov, "Strong plasmonic enhancement of photovoltage in graphene," Nat. Commun. **2**, 458 (2011).
16. O. M. Maragò, F. Bonaccorso, R. Saija, G. Privitera, P. G. Gucciardi, M. A. Iatì, G. Calogero, P. H. Jones, F. Borghese, P. Denti, V. Nicolosi, and A. C. Ferrari, "Brownian motion of graphene," ACS Nano **4**, 7515–7523 (2010).
17. M. Liu, X. Yin, E. Ulin-Avila, B. Geng, T. Zentgraf, L. Ju, F. Wang, and X. Zhang, "A graphene-based broadband optical modulator," Nature **474**, 64–67 (2011).
18. J. Niu, Y. J. Shin, Y. B. Lee, J. H. Ahn, and H. S. Yang, "Graphene induced tunability of the surface plasmon resonance," Appl. Phys. Lett. **100**, 061116 (2012).
19. F. Bonaccorso, Z. Sun, T. Hasan, and A. C. Ferrari, "Graphene photonics and optoelectronics," Nat. Photonics **4**, 611–622 (2010).
20. Z. Shi, L. Gan, T. H. Xiao, H. L. Guo, and Z. Y. Li, "All-optical modulation of a graphene-cladded silicon photonic crystal cavity," ACS Photon. **2**, 1513–1518 (2015).
21. W. B. Lu, W. Zhu, H. J. Xu, Z. H. Ni, Z. G. Dong, and T. J. Cui, "Flexible transformation plasmonics using graphene," Opt. Express **21**, 10475–10482 (2013).
22. T. H. Xiao, L. Gan, and Z. Y. Li, "Graphene surface plasmon polaritons transport on curved substrates," Photon. Res. **3**, 300–307 (2015).
23. P. Y. Chen, J. Soric, and A. Alù, "Invisibility and cloaking based on scattering cancellation," Adv. Mater. **24**, OP281–OP304 (2012).
24. B. Zhu, G. Ren, Y. Gao, Y. Yang, Y. Lian, and S. Jian, "Graphene-coated tapered nanowire infrared probe: a comparison with metal-coated probes," Opt. Express **22**, 24096–24103 (2014).
25. Y. Gao, G. Ren, B. Zhu, J. Wang, and S. Jian, "Single-mode graphene-coated nanowire plasmonic waveguide," Opt. Lett. **39**, 5909–5912 (2014).
26. J. S. Lee, S. I. Kim, J. C. Yoon, and J. H. Jang, "Chemical vapor deposition of mesoporous graphene nanoballs for supercapacitor," ACS Nano **7**, 6047–6055 (2013).
27. J. Kim, H. Son, D. J. Cho, B. Geng, W. Regan, S. Shi, K. Kim, A. Zettl, Y. R. Shen, and F. Wang, "Electrical control of optical plasmon resonance with grapheme," Nano Lett. **12**, 5598–5602 (2012).
28. J. P. Barton, D. R. Alexander, and S. A. Schaub, "Internal and near-surface electromagnetic fields for a spherical particle irradiated by a focused laser beam," J. Appl. Phys. **64**, 1632–1639 (1988).
29. L. A. Falkovsky and A. A. Varlamov, "Space-time dispersion of graphene conductivity," Eur. Phys. J. B **56**, 281–284 (2007).
30. L. A. Falkovsky, in *Optical Properties of Graphene* (IOP Publishing, 2008), p 012004.
31. J. P. Barton, D. R. Alexander, and S. A. Schaub, "Theoretical determination of net radiation force and torque for a spherical particle illuminated by a focused laser beam," J. Appl. Phys. **66**, 4594–4602 (1989).
32. J. P. Barton and D. R. Alexander, "Fifth-order corrected electromagnetic field components for a fundamental Gaussian beam," J. Appl. Phys. **66**, 2800–2802 (1989).
33. J. Chen, M. Badioli, P. Alonso-González, S. Thongrattanasiri, F. Huth, J. Osmond, M. Spasenović, A. Centeno, A. Pesquera, P. Godignon, A. Z. Elorza, N. Camara, F. J. García de Abajo, R. Hillenbrand, and F. H. L. Koppens, "Optical nano-imaging of gate-tunable graphene plasmons," Nature **487**, 77–81 (2012).
34. C. F. Chen, C. H. Park, B. W. Boudouris, J. Horng, B. Geng, C. Girit, A. Zettl, M. F. Crommie, R. A. Segalman, S. G. Louie, and F. Wang, "Controlling inelastic light scattering quantum pathways in graphene," Nature **471**, 617–620 (2011).
35. D. K. Efetov and P. Kim, "Controlling electron-phonon interactions in graphene at ultrahigh carrier densities," Phys. Rev. Lett. **105**, 256805 (2010).
36. F. H. L. Koppens, D. E. Chang, and F. J. García de Abajo, "Graphene plasmonics: A platform for strong light matter interactions," Nano Lett. **11**, 3370–3377 (2011).
37. B. R. Johnson, "Theory of morphology-dependent resonances: shape resonances and width formulas," J. Opt. Soc. Am. A **10**, 343–352 (1993).
38. Y. Yang, W. P. Zang, Z. Y. Zhao, and J. G. Tian, "Morphology-dependent resonance of the optical forces on Mie particles in an Airy beam," Opt. Express **21**, 6186–6195 (2013).